Journal of Controlled Release 347 (2022) 425–434

Contents lists available at ScienceDirect

Journal of Controlled Release

journal homepage: www.elsevier.com/locate/jconrel

Nanoparticle combination for precise stroma modulation and improved delivery for pancreatic cancer

Mubin Tarannum [a,b,1], Katherine Holtzman [c], Didier Dréau [c,d], Pinku Mukherjee [c,d], Juan L. Vivero-Escoto [a,b,d,*]

[a] Department of Chemistry, University of North Carolina Charlotte, Charlotte, NC 28223, USA
[b] Nanoscale Science Program, University of North Carolina Charlotte, Charlotte, NC 28223, USA
[c] Department of Biological Sciences, University of North Carolina Charlotte, Charlotte, NC 28223, USA
[d] Center for Biomedical Engineering and Science, University of North Carolina Charlotte, Charlotte, NC 28223, USA

ARTICLE INFO

Keywords:
Pancreatic cancer
Tumor stroma
Mesoporous silica nanoparticles
Combination therapy
SHh inhibitor

ABSTRACT

Therapeutic success in the treatment of pancreatic ductal adenocarcinoma (PDAC) is hindered by the extensive stroma associated to this disease. Stroma is composed of cellular and non-cellular components supporting and evolving with the tumor. One of the most studied mediators of cancer cell-stroma crosstalk is sonic hedgehog (SHh) pathway leading to the intense desmoplasia observed in PDAC tumors. Herein, we demonstrate that the use of mesoporous silica nanoparticles (MSNs) containing an SHh inhibitor, cyclopamine (CyP), and the combination of chemotherapeutic drugs (Gemcitabine (Gem)/cisplatin (cisPt)) as the main delivery system for the sequential treatment led to the reduction in tumor stroma along with an improvement in the treatment of PDAC. We synthesized two versions of the MSN-based platform containing the SHh inhibitor (CyP-MSNs) and the drug combination (PEG-Gem-cisPt-MSNs). In vitro and in vivo protein analysis show that CyP-MSNs effectively inhibited the SHh pathway. In addition, the sequential combination of CyP-MSNs followed by PEG-Gem-cisPt-MSNs led to effective stromal modulation, increased access of secondary PEG-Gem-cisPt-MSNs at the tumor site, and improved therapeutic performance in HPAF II xenograft mice. Taken together, our findings support the potential of drug delivery using MSNs for stroma modulation and to prevent pancreatic cancer progression.

1. Introduction

Pancreatic ductal adenocarcinoma (PDAC) has a poor prognosis with a 5-year survival rate of 9%. Moreover, this dismal prognosis is further reduced to 3% for patients diagnosed with advanced disease [1–3]. Several factors explain the therapeutic failure in PDAC including late detection, lack of biomarkers, aggressive local invasion, early metastatic nature, and resistance to systematic therapies. In particular, the presence of desmoplastic stroma that can account for up to 80–90% of the tumor volume, contributes to the chemotherapeutic resistance in PDAC [4,5]. PDAC stroma is composed of cellular and acellular components, including pancreatic stellate cells (PSCs), cancer-associated fibroblasts (CAFs), immune cells, and increased extracellular matrix (ECM) [6,7]. A highly desmoplastic stroma results in poor perfusion of systemic drugs and also acts as a physical barrier challenging nanoparticulate drug delivery system. Moreover, stroma-tumor crosstalk builds a unique tumor microenvironment (TME) that accelerates tumor progression, immune suppression, and metastasis [6,8].

While mostly quiescent in the healthy pancreas, the Sonic Hedgehog (SHh) pathway is aberrantly activated during PDAC tumorigenesis. The SHh pathway has been extensively studied for its role in cancer cell-stroma crosstalk leading to dense stroma deposition and has been assessed as a key target to limit stromal remodeling in PDAC. SHh binds both autocrine and paracrine i.e., on cancer cells and stromal cells, respectively. The later leads to desmoplasia; whereas former leads to tumor cell proliferation and metastasis [9–11]. Indeed, in pre-clinical models, the inhibition of SHh pathway by small-molecule antagonists such as cyclopamine (CyP), vismodegib (GDC-0449), or IPI-926 suppressed cancer cell proliferation, decreased stroma, and improved chemotherapy [12,13]. However, clinical trials using SHh inhibitors combined with chemotherapy led to negative or equivocal survival benefit when compared to chemotherapy alone [14,15]. The lack of

* Corresponding author at: Department of Chemistry, University of North Carolina Charlotte, Charlotte, NC 28223, USA.
E-mail address: jviveroe@uncc.edu (J.L. Vivero-Escoto).
[1] Current address: Dana-Farber Cancer Institute, Boston MA 02215, U.S.A.

https://doi.org/10.1016/j.jconrel.2022.05.019
Received 8 November 2021; Received in revised form 5 May 2022; Accepted 9 May 2022
Available online 19 May 2022

success in these clinical trials may be due to a number of factors including the bioavailability of SHh inhibitors at the tumor site; the toxicity of the treatment to the healthy organs; and the massive stromal depletion associated with the high dosage of SHh inhibitors [16]. Therefore, the use of drug delivery systems can potentially increase the targetability, the circulation of drugs, and bioavailability of SHh inhibitors in the tumor site.

The use of nanoparticles for the delivery of SHh inhibitors provides the following advantages: (i) Safe and efficient delivery mode reducing side effects and improving bioavailability, and (ii) it allows fine-tuning of the dose and time-dependent release of SHh inhibitor and chemotherapy agents to remodel the stroma while preserving tumor-restraining functions of the stroma [17,18]. Indeed, appropriately designed therapeutic regimens provide spatial and temporal access to the target while avoiding deleterious stromal depletion [16]. SHh pathway inhibitors including vismodegib and CyP have been loaded in the nanoparticles. These nanoplatforms have also been combined with other chemotherapy agents to improve the therapeutic outcome [16,19]. Karaca et al. [19] demonstrated that mixed micelle formulation of vismodegib and gemcitabine (Gem) triggered SHh inhibition and prevented pancreatic cancer proliferation in vitro and in vivo. In addition, Zhao et al. [16] showed the benefit of simultaneous delivery of CyP and the chemotherapy agent paclitaxel using a polymeric micelle formulation. The nanoformulation effectively modulated the tumor stroma by decreasing hypoxia while maintaining the tumor-restraining growth.

Mesoporous silica nanoparticles (MSNs) are versatile materials that can be selectively modified by adding various chemical functionalities either on internal or external surfaces facilitating specific drug control release [20–26]. Herein, we hypothesized that treatments using MSNs as

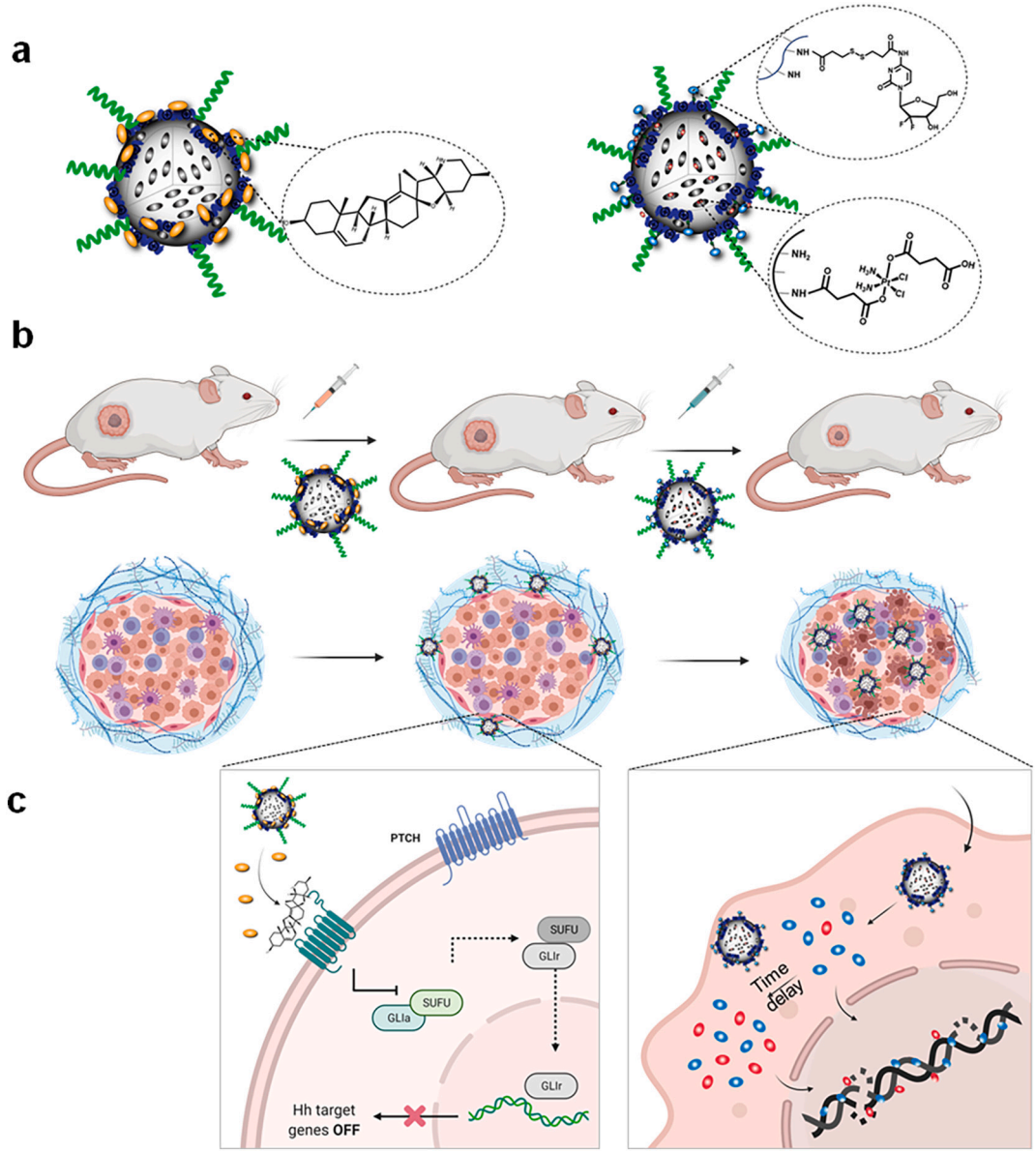

Fig. 1. Graphical Summary: (a) Schematic representation of the CyP-MSNs and PEG-Gem-cisPt-MSNs. CyP is loaded to the surface of MSNs using molecular interactions; whereas, Gem and cisPt are chemically conjugated to the external and internal surface of MSNs, respectively. (b) The sequential delivery using CyP-MSNs followed by PEG-Gem-cisPt-MSNs targets first the stroma via the interaction of CyP with stromal cells resulting in the SHh pathway inhibition, which allows a higher penetration of PEG-Gem-cisPt-MSNs in the tumor site. (c) MSNs deliver CyP outside of the stromal cells to trigger the inhibition of the SHh pathway. In addition, the synergistic action of Gem/cisPt owing to the nanoengineered deign and in situ differential release results in significant inhibition of PDAC tumor progression. Illustration created using BioRender.com

the main carrier for a sequential delivery of CyP and then of the chemotherapeutic combination Gemcitabine (Gem)/cisplatin (cisPt) would impact the stroma, improve the drug delivery and thus inhibit PDAC progression. Gem remains the clinical standard of care for the treatment of PDAC [27]. Recent insights gained from the characterization of recurrent genetic alterations revealed that a subset of PDACs, linked to germline-based mutations, can benefit from Pt-based agents such as cisPt, oxaliplatin or others. Therefore, Gem/cisPt is a promising combination to improve the therapeutic effect against PDAC [28–30]. Time-staggered delivery of each MSN carrier may optimize the release of drugs to specific tumor compartments; thereby, leading to effective stromal modulation, increased access of PEGylated Gem-cisPt-MSNs (PEG-Gem-cisPt-MSNs) at the tumor site and improved therapeutic performance (Fig. 1).

Here, we synthesize and characterize CyP-MSNs and PEG-Gem-cisPt-MSNs and demonstrate the inhibition capacity of CyP-MSNs against the SHh pathway in PDAC cells. We have recently demonstrated the remarkable therapeutic benefit of PEG-Gem-cisPt-MSNs in PDAC cells and in vivo models [26]. The combination of CyP-MSNs with PEG-Gem-cisPt-MSNs showed no cytotoxic effect on the PDAC cells when tested in vitro because of the low concentration of CyP-MSNs chosen to block the crosstalk between PDAC and stromal cells. In vivo investigations of safety, biodistribution, and therapeutic efficacy of the sequential combination of CyP-MSNs plus PEG-Gem-cisPt-MSNs were conducted in HPAF II xenograft mice. Tumors in the sequential therapy group demonstrated significant inhibition in tumor growth and stroma remodeling compared to tumors treated with PEG-Gem-cisPt-MSNs only, CyP-MSNs plus free Gem/cisPt, and control tumors. These results support further investigation of MSN-based drug delivery platforms for the precise delivery of anti-tumor agents for treatment of pancreatic and other cancers.

2. Experimental methods

2.1. Synthesis and characterization of PEG-Gem-cisPt-MSNs and CyP-MSNs

The experimental protocols and methods for the synthesis and characterization of PEG-Gem-cisPt-MSNs have been recently published [26]. The synthetic procedures for the CyP-MSNs are described in ESI.

2.2. Cytotoxic effect in PDAC cells

The cytotoxicity of individual MSN materials was tested as follows. HPAF II and MiaPaca-2 cells were seeded in 96-well plate at a cell density of 1000 cells per well. The cells were incubated for 24 h and then inoculated with different MSN materials (PEG-PEI-MSNs or CyP-MSNs) at increasing concentration (1–100 μg/mL). The MSNs were prepared in complete cell culture media and cells were treated for 72 h. The cells were then washed once with PBS, replaced with fresh media and incubated for another 24 h for recovery. Finally, the cells were washed once with PBS, and cell viability was evaluated using MTS assay. For MTS assay, 20 μL of the CellTiter 96® solution was added to each well containing 100 μL media. The cells were incubated for 2.5–3.5 h depending on the cell type, and the absorbance was measured at 490 nm using a Multiskan FC plate reader.

The cytotoxicity of the sequential combination of CyP-MSNs and PEG-Gem-cisPt-MSNs was tested as follows. HPAF II and MiaPaca2 cells were seeded in 96-well plate at a density of 1000 cells per well and incubated for 24 h. Then, the cells were inoculated with CyP-MSNs (10 μg/mL = CyP 4.4 μg/mL). The cells were treated with CyP-MSNs for 24 h. The cells were then washed with PBS and inoculated with increasing concentrations of PEG-Gem-cisPt-MSNs (1–100 μg/mL) for 48 h. Post treatment, the cells were washed once with PBS, replaced with fresh media and incubated for another 24 h for recovery. Finally; the cells were washed once with PBS and cell viability was evaluated using MTS assay, as described in the previous section. As a control group, treatment with only PEG-Gem-cisPt-MSNs was carried out.

2.3. Protein analysis for the inhibition of SHh pathway

HPAF II and MiaPaca-2 cells were seeded in 6-well tissue culture plates at a cell density of 100,000 cells per well. After a 24 h (37 °C, 5% CO_2, >95% humidity) incubation in DMEM supplemented with 10% FBS, antibiotic and antifungal, cells were further incubated with 40 μg/mL of MSN materials tested (PEG-PEI-MSNs or CyP-MSNs) suspended in cell culture media. After 72 h, both supernatants and cells were collected. Supernatants were assessed for the presence of SHh, a ligand released by cells. Collected cells were lysed in T-PER (ThermoFisher) supplemented with an EDTA-free protease inhibitor cocktail and mixed with Pro-Prep (2:1; Intron Biotechnology) for the analysis of PTCH1 and Gli1 expressions.

Briefly, after conducting a BCA assay on the cell lysates, lysates were further solubilized through the addition of and incubation with SDS (0.125% vol. final) for 15 min. Both supernatants (50 μL) and 50 μg of each cell lysate were loaded onto 0.45 μm nitrocellulose membranes using a dot-blot apparatus. Blots were incubated with Ponceau stain (Biorad) to verify protein loading and then blocked 3 h with 5% milk TBS tween 20 buffer and incubated overnight with diluted (1/500) primary antibodies against human PTCH1, Gli1 and SHh raised in mouse/hybridoma (Santa Cruz Biotechnology). Following an incubation with an anti-mouse HRP conjugated antibody (Jackson ImmunoResearch Laboratories), the presence of proteins was detected following incubation with chemiluminescence substrate (Biorad) and imaged using the ChemiDoc Imaging System (Biorad). Chemiluminescence intensity was quantified using Image J and the protein array analyzer plugin (open source software, NIH) normalized to protein loading and expressed as % of controls.

2.4. Sequential therapy studies in HPAF II tumor-bearing xenograft mice

Mice bearing HPAF II tumors were randomly divided into 4 treatment groups ($n = 3$); PBS, CyP-MSNs followed by free drugs (Gem/cisPt), PEG-Gem-cisPt-MSNs alone, and CyP-MSNs followed by PEG-Gem-cisPt-MSNs. Tumor growth was monitored by caliper measurements of the tumors every alternate day. The primary treatment (CyP-MSNs, 5 mg/kg in PBS) were injected intratumorally (*i.t.*) followed by the secondary treatment of PEG-Gem-cisPt-MSNs (40 mg/kg in 100 μL of water) or free Gem/cisPt (9.52/2.05 mg/kg), which was injected intravenously (*i.v.*) 48 h post CyP-MSNs administration. The interval of 48 h between injections has been selected based on previous studies with this platform [26]. The treatment with primary CyP-MSNs followed by secondary PEG-Gem-cisPt-MSNs was referred to as the therapy cycle. The whole treatment consisted of a total of 5 therapy cycles with an additional 48 h-interval between each cycle. Control groups followed the same administration protocol; CyP-MSNs (*i.t.*) and PEG-Gem-cisPt-MSNs (*i.v.*). Tumor growth was monitored every other day using caliper measurements. On day 30 post cell implantation, mice were euthanized, and the major organs were collected including liver, lungs, kidneys, spleen, heart, and tumor. The fluorescence associated with each organ was evaluated using the IVIS imaging system. Portions of the organs and tumors were fixed in formalin for histological analysis. Portions of the tissue samples were frozen and used later to determine the Si and Pt content.

2.5. Statistical analysis

All the data is represented as mean ± SD unless mentioned otherwise. The hydrodynamic size and ζ-potential analysis were performed in triplicates. The amount of CyP complexed to the MSNs is reported as average of 3 independent batches. For the cell viability studies, the GraphPad Prism was used to calculate the IC_{50} values. For the in vivo

therapeutic experiments, tumor volumes were reported as mean ± SEM, and compared using two-way ANOVA with Tukey's multiple comparison test. Tumor weight difference between treatment groups were compared using one-way ANOVA or *t*-test. The NIR fluorescence, Si and Pt content in organs were reported as mean ± SEM and compared using Two-way ANOVA. All the statistical analyses were performed using GraphPad Prism (La Jolla California, CA, USA) with $\alpha = 0.05$ and reported as stars assigned to the *p* values; ****$p \leq 0.0001$, ***$p \leq 0.001$, **$p \leq 0.01$, *$p \leq 0.05$ and ns $p > 0.05$.

3. Results and discussions

3.1. Design of primary and secondary MSN carriers for the delivery of CyP and gem/cisPt

We investigated whether the time-staggered sequential delivery of SHh inhibitor and Gem/cisPt drugs using MSN carriers improve their delivery to specific tumor compartments. This approach should lead to effective stromal modulation, increased access of secondary PEG-Gem-cisPt-MSNs at the tumor site and overall improved therapeutic performance.

The primary MSN material was modified with PEI (MW = 1.8 KDa) and PEG (MW = 2.0 KDa) polymers on the external surface. This material was further complexed with the sonic hedgehog inhibitor, cyclopamine (CyP) (Fig. 2a). The synthetic approach relies on the molecular interaction between CyP molecules and PEI polymer on the surface of MSNs through H-bonding [31]. This strategy results in a quick release of CyP in the TME followed by its interaction with the Smoothened (SMO) receptors on the cancer cells and fibroblasts (Fig. 1b). Whereas the secondary MSN material carries the Gem/cisPt combination using a stimuli-responsive nanoengineered approach that has been optimized for spatio-temporal delivery of the drug combo inside tumor tissue (Fig. 1c) [26].

The primary nanocarrier (CyP-MSNs) was synthesized following the scheme depicted in Fig. 2a. The surface of MSNs was coated with PEI (MW = 1.8 KDa) via the electrostatic interaction of PEI with phosphonate groups previously grafted on the MSNs. PEI-MSNs were further conjugated with MeO-PEG-NHS (MW = 2.0 KDa) using coupling chemistry. Finally, CyP molecules were complexed to PEG-PEI-MSNs through molecular interactions. The hydrodynamic diameter (D_h) and surface charge of the MSNs, PEG-PEI-MSNs and CyP-MSNs were characterized using DLS and ζ-potential (Table S1 in ESI). CyP-MSNs exhibited a D_h of 252 ± 40 nm (PdI = 0.3) in PBS (Fig. 2b). The surface charge of the CyP-MSNs was almost neutral with a ζ-potential of 7.9 ± 0.7 mV compared to the PEG-PEI-MSNs, which exhibit a ζ-potential of 28 ± 1 mV in PBS as an indication of the functionalization of the surface with CyP (Fig. 2c). The amount of CyP molecules loaded onto MSNs was quantified using HPLC, the experimental protocol can be found in ESI. The loading data showed a high CyP amount of 44.7 wt% similar to the previous reports for MSNs [28]. The release of CyP molecules was investigated at low pH (6.0), mimicking the intratumoral acidic pH, and at physiological pH (7.4) in solution [29]. The release data indicate a clear burst release of the CyP inhibitor at pH 6.0 (Fig. S1), which corroborates that at low pH the presence of protons (H^+) disrupt the H-bonding between CyP and MSNs. On the contrary, a steady release of CyP at pH 7.4 was observed (Fig. S1).

For the synthesis of the secondary nanocarrier (PEG-Gem-cisPt-MSNs), the Gem/cisPt drugs were chemically conjugated to the MSNs. The selective functionalization of MSNs was achieved via the optimized multi-step procedure recently published by our group and is depicted in Fig. 2d [26]. The cisPt prodrug was conjugated to the interior surface of MSNs to afford cisPt-MSNs with 5.13 ± 0.9 wt% ($n = 3$) loading of cisPt as measured by ICP-MS. Whereas the Gem prodrug was conjugated to the surface of the MSNs via PEI polymer. This strategy afforded Gem-cisPt-MSNs with 23.9 ± 2.6 wt% Gem loading ($n = 5$) measured by UV–vis spectroscopy. The structural features of this nanomaterial such as hydrodynamic size (Dh), surface charge, TEM, N_2 isotherms, and drug content have been reported (Figs. 2e and S2) [26]. Importantly, the material design by selective localization of drugs led to an "*in situ* differential" release of Gem followed by cisPt, which afforded a synergistic effect between Gem and cisPt combination as shown previously [26]. This MSN platform offers several advantages for the co-delivery of Gem/cisPt drugs including stimuli-responsive delivery under reducing conditions, "in situ differential" drug release due to the location of the drugs in the MSNs, and controlled ratio of the drugs [26].

3.2. Inhibitory function and cytotoxicity of CyP-MSNs in PDAC cells

To demonstrate that CyP-MSNs maintain the inhibitory effects of the parent SHh inhibitor, we investigated the impact of the material on

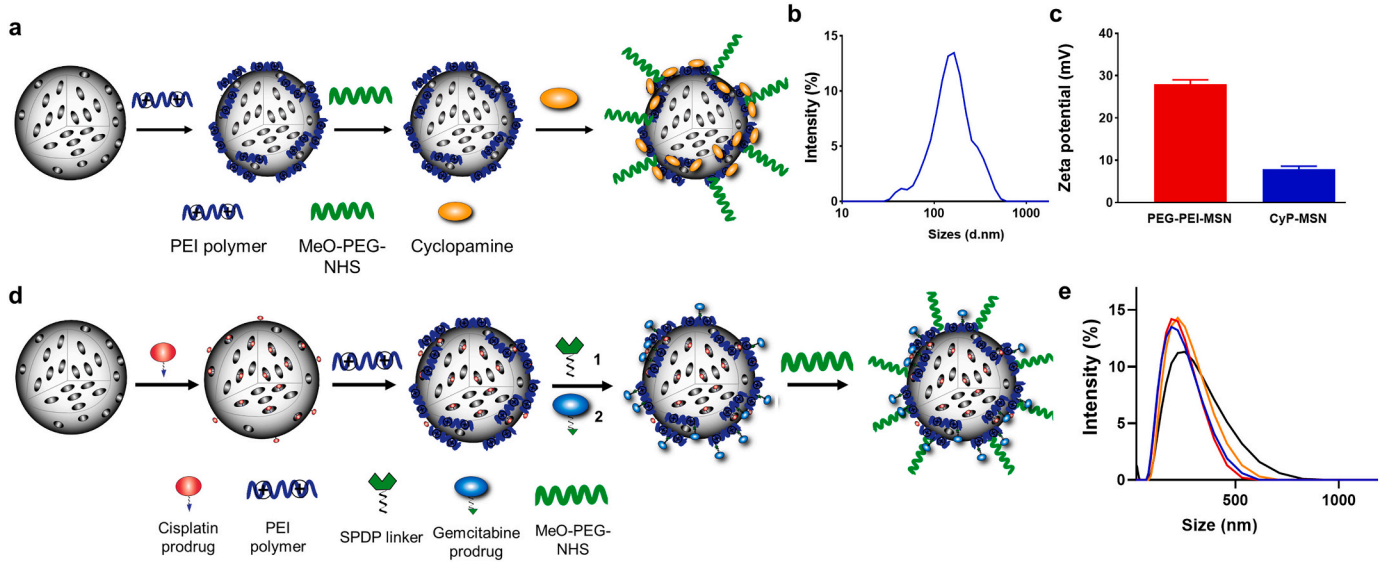

Fig. 2. Synthesis and characterization of CyP-MSNs and PEG-Gem-cisPt-MSNs. (a) Graphical representation of the synthesis of CyP-MSNs. (b) The particle size distribution (PSD) plot of CyP-MSNs in PBS. (c) ζ-potential of CyP-MSNs obtained using DLS ($n = 3$). (d) Graphical representation of the synthesis of PEG-Gem-cisPt-MSNs (modified from [26]). (e) The particle size distribution (PSD) plot of MSNs (blue), cisPt-MSN (red), Gem-cisPt-MSN (orange), and PEG-Gem-cisPt-MSNs (black) in PBS. (For interpretation of the references to colour in this figure legend, the reader is referred to the web version of this article.)

effector proteins in PDAC cells and the cytotoxicity of CyP-MSNs combined with PEG-Gem-cisPt-MSNs. PDAC cells are heterogenous with high variability in SHh expression, sensitivity to SHh inhibitors, and non-canonical SHh activation [32,33]. In particular, the non-canonical SHh activation in PDAC cells signals SHh downstream of SMO or PTCH receptors; hence, these cells do not respond to the SMO antagonists. PDAC cells including HPAF II, MiaPaca-2, and Capan-2 display enhanced SHh receptor expression and increased sensitivity to SHh inhibitors like CyP and vismodegib [32,33]. In contrast, PDAC cells such as BxPC3 and Panc-1 do not express the SHh receptors and show resistance to SHh inhibitors. Here, we used HPAF II and Miapaca-2 cells to test the inhibitory effect of CyP-MSNs.

Overexpression of SHh ligands and of related downstream markers i.e., smoothened receptor (SMO), patched receptor (PTCH1), glioma-associated oncogene homolog-1 (Gli1) are related to poor prognosis of PDAC (Fig. 3a). We assessed the effects of CyP-MSNs' treatment on the expression of these SHh markers i.e., SHh ligand, PTCH1 receptor and the downstream Gli1 transcription factor, to confirm the inhibitory ability of CyP-MSNs on the SHh pathway (Fig. 3). HPAF II and MiaPaca-2 cells were treated with CyP-MSNs for 72 h. The conditioned media was collected to analyze the secreted SHh ligand. The cells were lysed and analyzed for protein expression, PTCH1, and Gli1. Both PDAC cells showed low expression of PTCH1 and Gli1 indicating that CyP-MSNs efficiently inhibited the SHh pathway. The CyP-MSN treatment decreased SHh ligand expression in HPAF II cells, but not in MiaPaca-2 cells likely due to the different threshold responses to CyP-MSNs (Fig. 3b). These data demonstrated that CyP-MSNs maintain the inhibitory function of CyP and that CyP-MSNs permit CyP interaction with the SMO receptors on the cell surface and lead to an efficient inhibition of the SHh pathway.

The cytotoxic effect of CyP-MSNs against HPAF II and Miapaca-2 cells was determined using the MTS assay. Incubation with CyP-MSNs led to limited decrease in cell viability even at high concentration i.e., ~ 80% viable PDAC cells following incubation with 60 μg/mL (equivalent to 26.4 μg/mL of CyP) (Fig. 3c). Though autocrine function of SHh in PDAC cells increases cell proliferation and invasion, inhibiting the SHh pathway may not always contribute to the cell death, as cancer cells do not completely depend on the SHh mechanism for growth and proliferation. Therefore, usually very high concentrations of CyP are required to observe some cytotoxic effect.

To evaluate the combined therapeutic effect of both primary and secondary nanocarriers, a low dose of CyP-MSNs (10 μg/mL; CyP = 4.4 μg/mL) was used. This concentration was derived from the inhibitory and cytotoxic investigations of CyP-MSNs (see above). PEG-Gem-cisPt-MSN platform is designed to enhance the effects of the Gem/cisPt chemotherapy combination through spatiotemporal, ratiometric, and in situ differential release of Gem/cisPt (Fig. 1c). The HPAF II or Miapaca-2 cells were first treated with CyP-MSNs (10 μg/mL, 4.4 μg/mL) for 24 h, i.

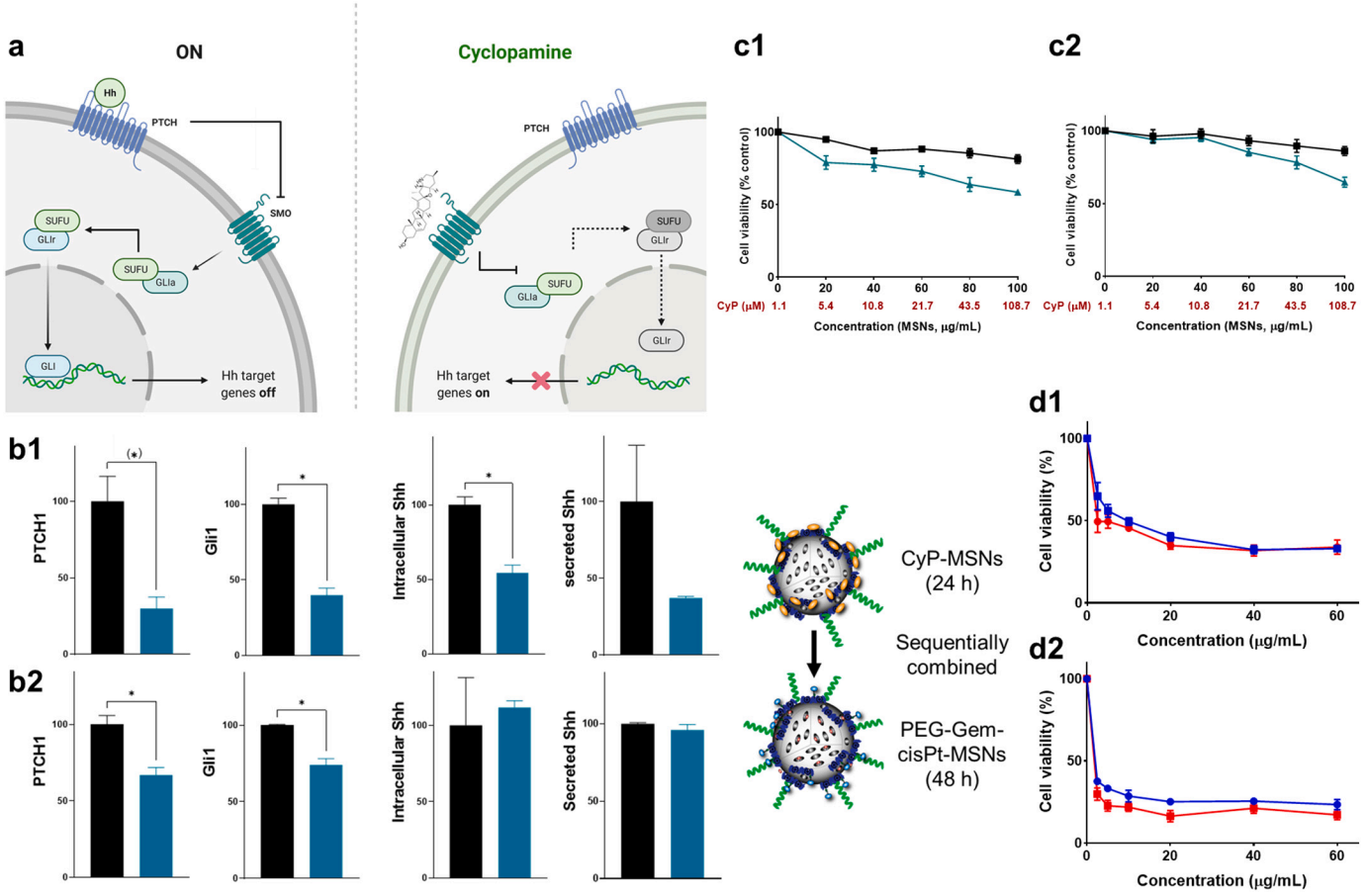

Fig. 3. (a) Scheme of the inhibition of SHh pathway. The SHh ligand (Hh) released from the cancer cells binds to the transmembrane protein receptor PTCH, which relieves smoothened (SMO) from the inhibitory effect of PTCH. Subsequently, SMO causes the translocation of Gli to the nucleus and activates several Gli-induced transcriptional effectors; paracrine activation leads to desmoplasia; whereas the autocrine activation leads to tumor cell proliferation and metastasis. Inhibitory effects of CyP-MSNs on PDAC cells, HPAF II (b1) and MiaPaca-2 (b2). Cells were treated with PEG-PEI-MSNs (black) or CyP-MSNs (green) for 72 h and protein analysis was performed to quantify SHh ligand, PTCH1 and Gli1. Cytotoxic effect of CyP-MSNs on HPAF II (c1) and MiaPaca (c2). Cytotoxic effect of sequential combination of CyP-MSNs and PEG-Gem-cisPt-MSNs (red) or PEG-Gem-cisPt-MSNs alone (blue) on PDAC cells, HPAF II (d1) and MiaPaca-2 (d2). Unpaired *t*-test was performed between different groups to determine the statistical difference. Statistics: ****$p \leq 0.0001$, ***$p \leq 0.001$, ** $p \leq 0.01$, * $p \leq 0.05$ and (*) $0.05 < p < 0.1$. (For interpretation of the references to colour in this figure legend, the reader is referred to the web version of this article.)

e., the primary treatment. The cells were then inoculated for 48 h with increasing concentrations of PEG-Gem-cisPt-MSNs, i.e., the secondary treatment. The cytotoxicity of PEG-Gem-cisPt-MSNs was not significantly different with or without the primary treatment using CyP-MSNs possibly due to the low dose of CyP-MSNs used (Fig. 3d). In addition, the primary treatment aims to inhibit the SHh pathway and may not necessarily have a cytotoxic effect.

3.3. Therapeutic efficacy of the sequential combination of CyP-MSNs and PEG-Gem-cisPt-MSNs in HPAF II xenograft mice

The combination of CyP-MSNs and PEG-Gem-cisPt-MSNs were tested in the human HPAF II cell xenograft model. Human HPAF II cells express the SHh pathway and HPAF II xenograft model tumors have shown to recruit stromal components [34]. Four treatment groups were assessed (administration scheme Fig. 4a); PBS, CyP-MSNs followed by free drugs, PEG-Gem-cisPt-MSNs alone, and CyP-MSNs followed by PEG-Gem-cisPt-MSNs. Mice bearing ~100 mm^3 HPAF II tumors were intratumorally injected with CyP-MSNs (5 mg/kg) followed by intravenous injection of PEG-Gem-cisPt-MSNs (40 mg/kg) for a total of 5 treatment cycles. Tumor volumes were measured over the course of treatment. CyP-MSNs were not injected in the first cycle to avoid the risk of stromal ablation. Moreover, the low concentration of CyP used here have been demonstrated to selectively inhibit the SHh pathway and limit stroma deposition without causing stroma depletion in the PDAC tumors [16].

Tumor volumes were similar in mice treated with CyP-MSNs followed by free Gem/cisPt compared to control mice (Fig. 4b). In contrast, tumors treated with PEG-Gem-cisPt-MSNs grew more slowly compared to PBS tumors ($p < 0.05$). The greatest tumor inhibition was observed in mice treated with CyP-MSNs followed by PEG-Gem-cisPt-MSNs ($p < 0.0001$). At the endpoint, the tumors were harvested and weighed to corroborate the therapeutic efficacy of the sequential therapy. The tumors were 71.3% smaller for CyP-MSNs plus PEG-Gem-cisPt-MSNs, 47.6% for PEG-Gem-cisPt-MSNs alone, and 15.2% for CyP-MSNs plus free Gem/cisPt tumors in comparison to the non-treatment group, based on the tumor weight measurements (Fig. 4c). The impact of CyP-MSNs' pretreatment on the improvement of secondary PEG-Gem-cisPt-MSNs was investigated by fluorescence and Pt analysis in the tumors. This showed both increased fluorescent intensity and Pt content in the tumors when pretreated with CyP-MSNs compared to PEG-Gem-cisPt-MSNs alone (Fig. S3). These data together with the enhanced therapeutic performance as evidenced from the tumor volumes and weights, is a clear indication that CyP-MSNs increased the penetration of PEG-Gem-cisPt-MSNs in tumor tissue. These results highlight that the MSN carrier efficiently delivered CyP and Gem/cisPt where the pretreatment with CyP-MSNs significantly increased the therapeutic benefit of PEG-Gem-cisPt-MSNs. The data also suggest that this dramatic improvement in therapeutic efficacy results from the combination of the SHh inhibition directly impacting the tumor stroma, allowing for more PEG-Gem-cisPt-MSNs to extravasate to the PDAC cells.

3.4. Analysis of SHh pathway inhibition and tumor microenvironment changes

To understand the impact of the sequential treatment on the tumor cells and TME, we determined the effect of the different experimental groups on SHh pathway by analyzing the protein expression of SHh ligand, PTCH1, and Gli1 in the tumor lysate (Fig. 5a). The decreased protein expression associated with CyP-MSNs plus free drugs treatment compared with the PBS group ($p < 0.01$) demonstrate that MSNs

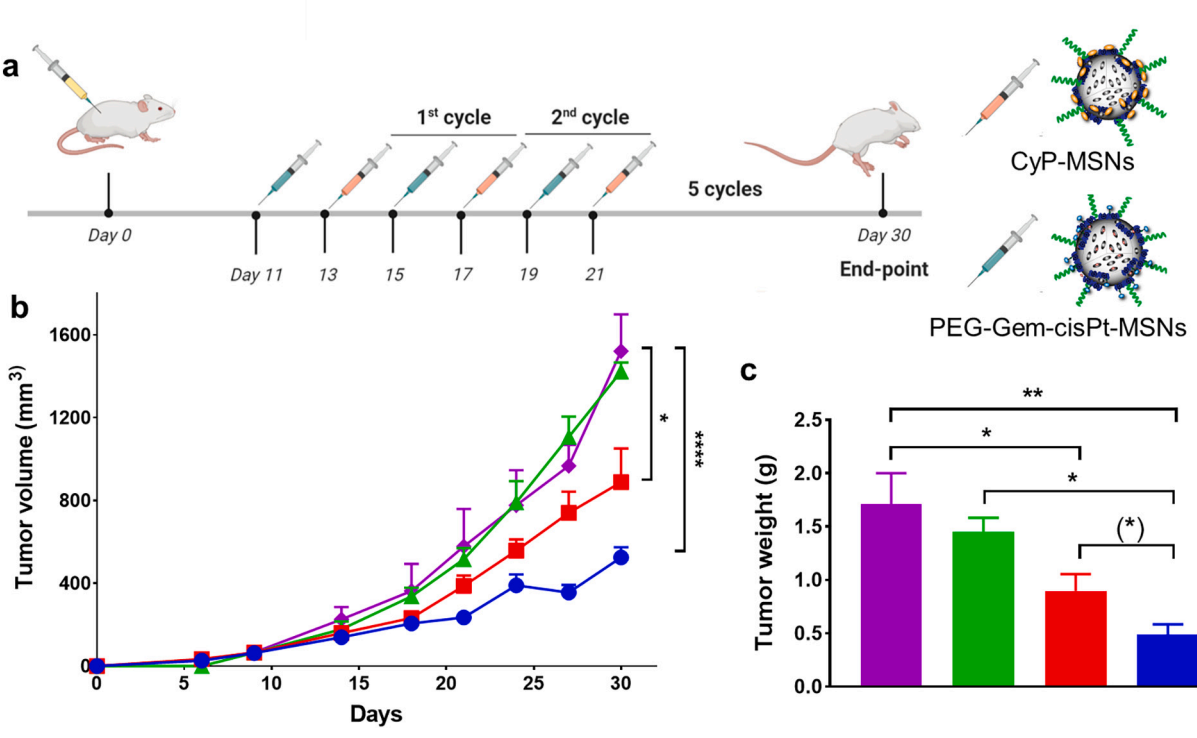

Fig. 4. Therapeutic study of CyP-MSNs plus PEG-Gem-cisPt-MSNs in the HPAF II bearing xenograft mice. (a) Schematic representation of the treatment regimen; HPAF II cells were subcutaneously implanted in NSG mice and the treatment started 11 days post cell implantation. (b) Tumor volume measurement of mice in different treatment groups: PBS (purple diamonds), CyP-MSNs plus free drugs (green upward triangles), PEG-Gem-cisPt-MSNs (red squares), and CyP-MSNs plus PEG-Gem-cisPt-MSNs (blue circles) ($n = 3$ mice per group). Two-way ANOVA was performed between different groups and time points to compare treatment groups. (c) Tumor weights measured at the endpoint: PBS (purple), CyP-MSNs plus free drugs (green), PEG-Gem-cisPt-MSNs (red), and CyP-MSNs plus PEG-Gem-cisPt-MSNs (blue) (n = 3 mice per group). One-way ANOVA with Tukey's multiple comparisons were used to access differences: ****$p \leq 0.0001$, ***$p \leq 0.001$, ** $p \leq 0.01$, * $p \leq 0.05$ and ns $p > 0.05$ between treatments and *t*-test analysis to test difference between CyP-MSNs and PEG-Gem-cisPt-MSNs: (*) $p \leq 0.05$. (For interpretation of the references to colour in this figure legend, the reader is referred to the web version of this article.)

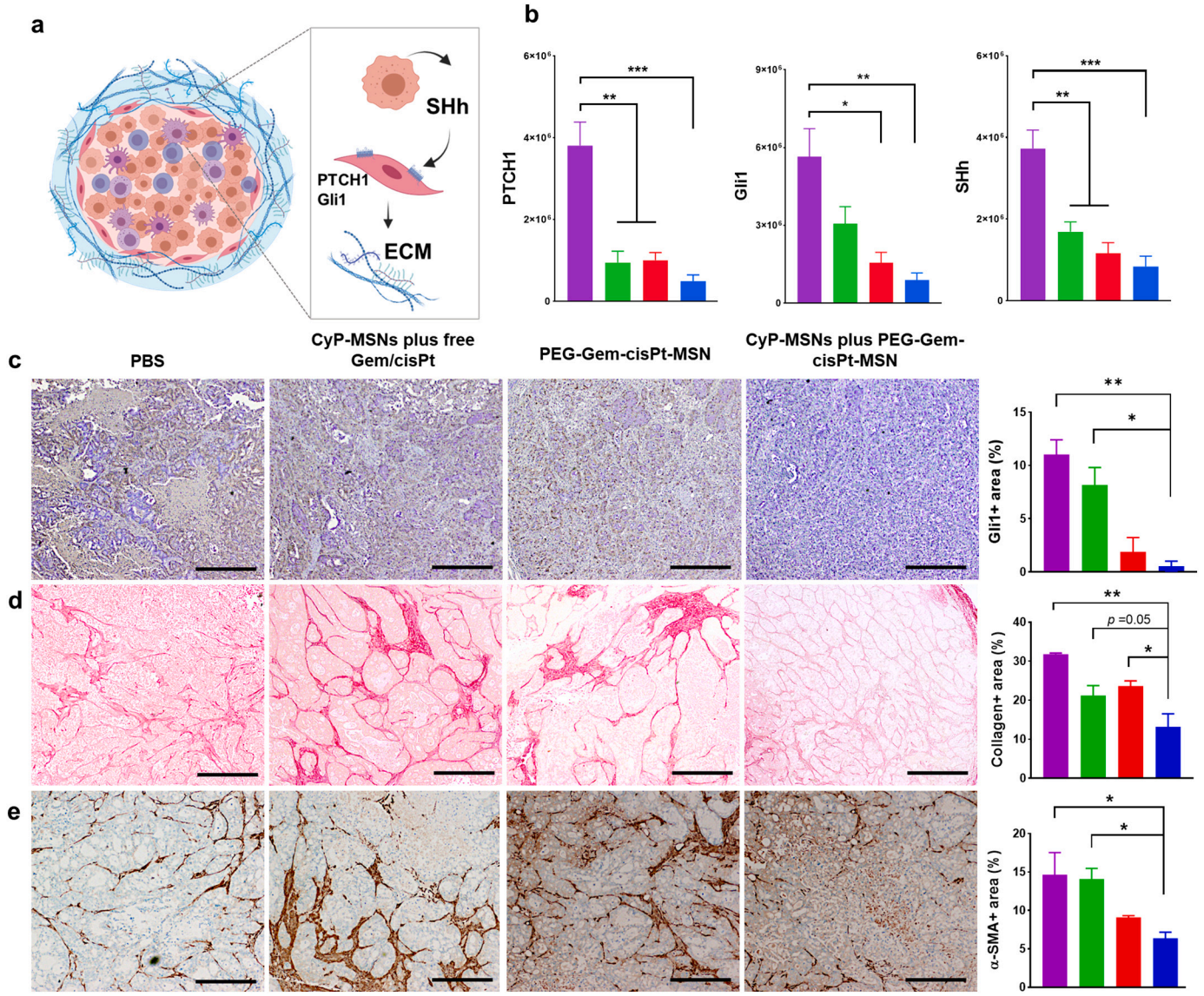

Fig. 5. SHh pathway and tumor microenvironment changes post treatment with CyP-MSNs plus PEG-Gem-cisPt-MSNs. (a) Schematic of complex tumor-stroma crosstalk mediated by SHh pathway. (b) Protein analysis of tumor lysate for SHh pathway markers: PBS (purple), CyP-MSNs plus free drugs (green), PEG-Gem-cisPt-MSNs (red), and CyP-MSNs plus PEG- Gem-cisPt-MSNs (blue) (n = 3 mice per group). (c) Ex vivo analysis of tumor sections stained for Gli protein and quantification. (d) Ex vivo analysis of tumor sections stained with picrosirius red for collagen content analysis after treatment. (e) Ex vivo analysis of tumor sections stained for α-SMA expression after treatment. Differences between groups were tested using one-way ANOVA. ****$p \leq 0.0001$, ***$p \leq 0.001$, ** $p \leq 0.01$, * $p \leq 0.05$ and ns $p > 0.05$. Scale bar = 1 mm. (For interpretation of the references to colour in this figure legend, the reader is referred to the web version of this article.)

efficiently transported and delivered CyP molecules in the tumor tissue. These results further corroborate that the poor therapeutic efficacy observed for this treatment group is due to the limited bioavailability of the chemo drugs in the tumor tissue. The treatment with PEG-Gem-cisPt-MSNs alone seems to also have an impact on the SHh pathway; possibly related to decreased HPAF II tumor cells. The sequential combination CyP-MSNs plus PEG-Gem-cisPt-MSNs led to the highest decrease in SHh ligand, PTCH1, and Gli1 protein expressions ($p \leq 0.001$) (Fig. 5b); which is a direct effect of the CyP inhibitor delivered by MSNs on the SHh pathway accompanied by the effective killing of tumor cells by PEG-Gem-cisPt-MSNs. These observations were confirmed by IHC staining for Gli1 expression. The Gli1+ area in tumors showed significant inhibition in the CyP-MSNs plus PEG-Gem-cisPt-MSNs group compared to PBS group ($p < 0.01$) and CyP-MSN plus free drugs ($p < 0.05$) (Fig. 5c).

Next, we investigated the effect of sequential treatment on the tumor stroma in particular extracellular matrix deposition, a hallmark of PDAC [16]. Tumor sections from each treatment group were stained with picrosirius red stain to evaluate collagen content (Fig. 5d) [35]. The collagen content in the tumor tissue was decreased and had an even spatial distribution following the sequential combination of CyP-MSNs plus PEG-Gem-cisPt-MSNs. In contrast, tumors collected from the other treatment groups presented more heterogeneous distribution of collagen deposition characteristic of PDAC tumors. Collagen+ area in the tumor section was least in CyP-MSNs plus PEG-Gem-cisPt-MSNs as compared PBS ($p < 0.01$) and PEG-Gem-cisPt-MSN group ($p < 0.05$) (Fig. 5d) [4]. These data highlight that the sequential treatment with CyP-MSNs plus PEG-Gem-cisPt-MSNs drastically reduced collagen deposition and thus significantly altered the tumor ECM ($p < 0.01$ compared to PBS). To further corroborate this observation, tumor tissues were stained for the cancer-associated fibroblast (CAF) marker smooth muscle α-actin (α-SMA) [36], a prognostic marker for many cancers including PDAC [37]. CAFs mainly activated from the normal resident tissue fibroblasts are abundant and play critical roles modulating the TME. As expected, the tumor α-SMA expression in sequential treatment

group was significantly less compared to other groups ($p < 0.05$ compared to PBS) and was correlated to the tumor collagen (Fig. 5e). This result confirms that the SHh pathway inhibition led to a decrease or normalization of CAF activities. Overall, time-staggered controlled delivery of CyP and Gem/cisPt using MSNs led to effective inhibition of the tumor cell-stromal communication, remodulation of TME that resulted in improved extravasation of chemotherapy agents.

3.5. *In vivo safety and biodistribution of sequential therapy*

The biocompatibility and safety of MSN platform has already been demonstrated in vivo by our group and others [26,38,39]. In this work MSNs were used as carrier for both primary and secondary treatments, increasing the probability of side-effects associated with the platform. Therefore, the safety of the sequential treatment was evaluated by monitoring the mice behavior and body weights during the treatment process, and by performing a histopathological investigation of the organs post treatment. No significant changes in body weights were observed in any of the treatment groups (Fig. S4a). Moreover, there was no behavioral changes noted during the treatment. The histopathological evaluation of major organs like liver, lungs, kidneys, and heart showed no significant signs of toxicity associated with the CyP-MSNs plus PEG-Gem-cisPt-MSNs and PEG-Gem-cisPt-MSNs treatment groups compared to the PBS group (Fig. 6). Several studies have shown that MSNs accumulate mainly in liver [40]; therefore, it is critical to investigate the liver function after treatment. Blood serum analysis show that the AST/ALT values obtained for the MSN materials were comparable to those for the PBS group, further corroborating the biocompatibility of the nanoparticles (Fig. S4b). These results confirmed that the MSNs are safe and biocompatible when used as sequential therapy. Morphological changes were observed in the kidney tissue from mice injected with CyP-MSNs plus free drugs (Fig. S5a). The increased off-target toxicity of Gem and cisPt in liver and kidney is well-documented and is one of the major side-effects of chemotherapy [41]. Quantitative analysis of Pt content in those organs show that treatment with free drugs led to the highest accumulation of Pt (Fig. S5b), a clear indication that the toxicity observed in the kidneys is most likely associated with cisPt. These data confirm our recent report showing the impact of MSNs on decreasing the accumulation of cisPt in kidney [26].

MSNs usually follow the hepatobiliary excretion pathway with main accumulation of the nanoparticles in the liver and spleen [26,38]. We analyzed the biodistribution of the MSNs by NIR fluorescence imaging and Si content using ICP-OES analysis of major organs. NIR fluorescence signaling indicates that MSNs are predominantly localized in spleen, liver and lungs (Figs. S6a and S6b). ICP-OES analysis of Si content correlates with the NIR fluorescence for the accumulation of MSNs in those organs (Fig. S6c). This confirms our previous observations and the slow clearance from the hepatobiliary system [26,39].

The therapeutic efficacy in HPAF II xenograft mice results suggest that the CyP-MSNs' pre-treatment inhibit the stroma-cancer cell interactions via inhibition of the SHh pathway. This, in turn, leads to stromal modulation, better penetration of the secondary nanoparticles into the tumor and delivery of chemotherapy agents Gem/cisPt to tumor cells. Increased fluorescence and Pt content were observed in tumors injected with primary CyP-MSN followed by PEG-Gem-cisPt-MSNs (Fig. S3), a result of the impact of CyP-MSNs on the accumulation of PEG-Gem-cisPt-MSNs. The activity and efficacy of the proposed MSNs staggered delivery of SHh inhibitor and Gem-cisPt combination is supported by ex vivo protein and IHC analysis.

4. Conclusions

One of the major hallmarks of PDAC is its desmoplastic stroma where the intricate crosstalk between cancer cells and stromal cells contributes

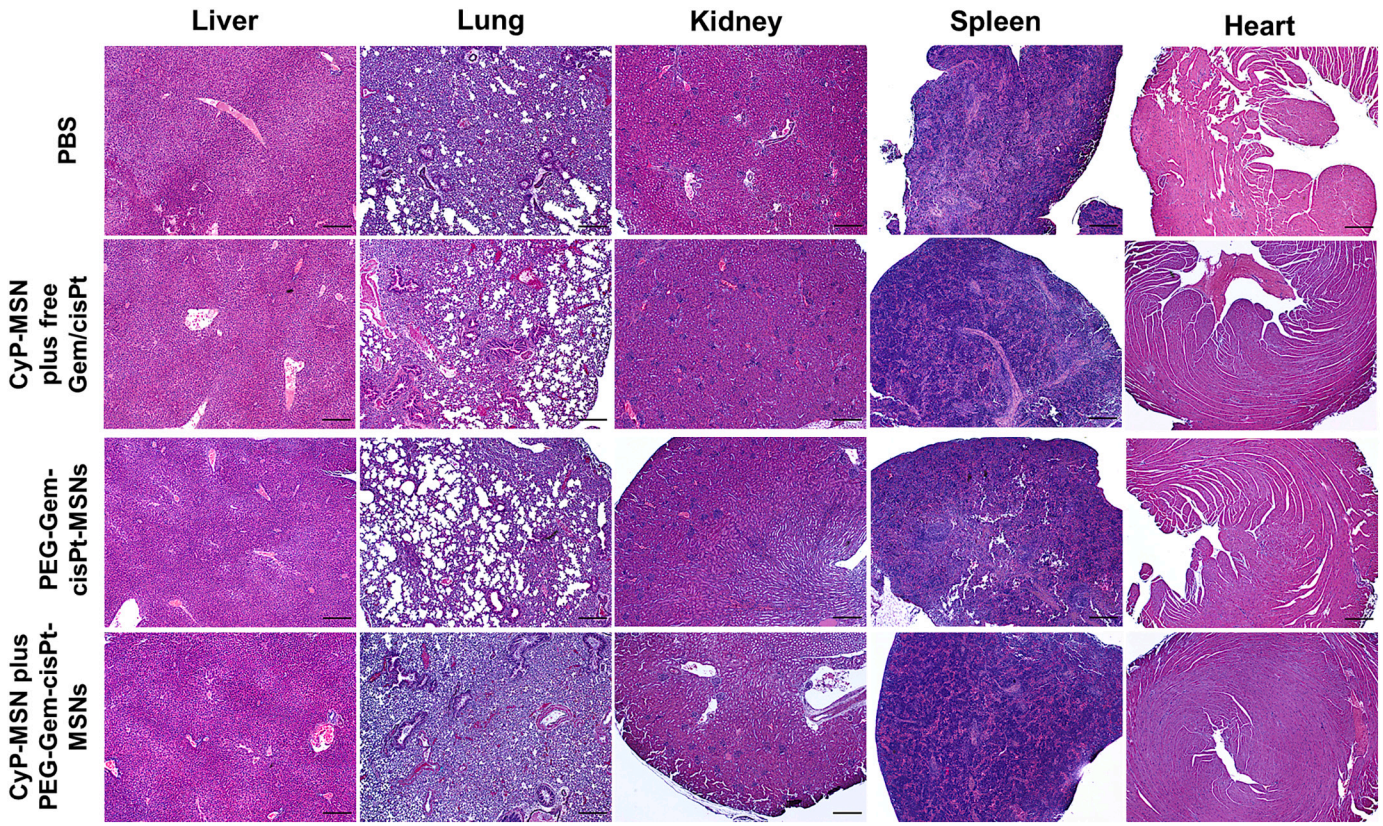

Fig. 6. Biosafety of the sequential treatment. H&E stained slides of liver, lungs, kidneys, spleen, and heart harvested from the mice after the therapeutic efficacy studies (Scale bars = 500 μm).

to tumor progression and metastasis. The stroma through its fibrotic extracellular matrix acts as a physical barrier preventing drug delivery, while also contributing to off-target toxicity of stromal cells thereby increasing tumor resistance. We designed an MSN-based sequential therapy for stroma modulation (CyP-MSNs) and the delivery of Gem/cisPt (PEG-Gem-cisPt-MSNs) chemotherapy to tumor cells. Our approach allows the control of time and spatial access of the SHh inhibitor and chemo drugs, which have different pharmacokinetics and targets in tumor tissues.

In vitro experiments in HPAF II and MiaPaca-2 cells highlight the effective inhibition of SHh pathway associated with CyP-MSNs as indicated by PTCH1, Gli1, and SHh protein expression. These results corroborate that MSNs can transport and deliver the SHh inhibitor to the cells. As intended, the combination therapy of CyP-MSNs plus PEG-Gem-cisPt-MSNs showed no cytotoxic effect on the HPAF II cells. Whereas there is a potential of using our combination to deplete the PDAC tumors of cancer stem-like cells, which overexpress SHh pathway and are responsible for resistance and recurrence. This aspect needs to be explored in the future.

In vivo evaluation of the sequential combination using CyP-MSNs plus PEG-Gem-cisPt-MSNs therapy in mice bearing the aggressive xenograft HPAF II tumor demonstrated the therapeutic efficacy of this approach. Tumor growth inhibition and decreased tumor weights at endpoint strongly support an improved delivery of the chemotherapy agents Gem/cisPt carried by MSNs to the tumor cells. In addition, tumor analysis indicated changes in tumor microenvironment as evidenced by collagen deposition and α-SMA expression. Further studies involving orthotopic and patient-derived xenograft preclinical mouse models mimicking the aggressive desmoplastic reaction of the PDAC tumors are warranted. Overall, the in vivo data presented here demonstrated that the MSN-based sequential combination strategy leads to reduced stroma fibrosis, allowing for improved delivery of Gem/cisPt to tumor cells, which results in an increased therapeutic efficacy in PDAC.

Author contributions

M.T. carried out laboratory research (design, acquisition, analysis and data interpretation) for the synthesis and characterization of MSN materials, in vitro and in vivo experiments; conceptualized and designed of the whole work; and wrote all versions of the manuscript.

K. H. did the laboratory research (design, acquisition, analysis and data interpretation) to determine the protein expression in vitro and in vivo associated with the SHh pathway following CyP-MSN treatment; and substantively revised the final version of the manuscript.

D.D. conceptualized and designed of the in vitro and in vivo work; participated in the acquisition of histological analyses, analyzed and interpreted the data; and substantively revised the final version of the manuscript.

P.M. conceptualized and designed of the in vivo work; analyzed and interpreted the data; and substantively revised the final version of the manuscript.

J.V.-E. conceptualized and designed of the whole work; analyzed and interpreted the data; and substantively revised all versions of the manuscript.

Funding sources

National Institute of Cancer of the National Institutes of Health under Award Number R15CA192160.

Acknowledgments

M. T. received financial support from the Thomas Reynolds Graduate Research Award. Work reported here was supported by the National Institute of Cancer of the National Institutes of Health under Award Number R15CA192160 (to J.V.-E. and P.M.). The content of this publication does not necessarily reflect the views or policies of the Department of Health and Human Services, nor does mention of trade names, commercial products, or organizations imply endorsement by the U.S. Government. Authors would also like to thank the vivarium staff; in particular, the veterinarian Dr. Chandra Williams at UNC Charlotte for assistance with animal experiments and data analysis. Finally, we thank Ms. Varsha Godakhindi, Ms. Hemapriyadarshini Vadarevu and Mr. Bryce Holmes for help with the TEM, CyP analysis and ICP-OES analysis, respectively.

Appendix A. Supplementary data

Supplementary data to this article can be found online at https://doi.org/10.1016/j.jconrel.2022.05.019.

References

[1] F. Bray, J. Ferlay, I. Soerjomataram, R.L. Siegel, L.A. Torre, A. Jemal, Global cancer statistics, GLOBOCAN estimates of incidence and mortality worldwide for 36 cancers in 185 countries, CA Cancer J. Clin. 68 (2018) (2018) 394–424.
[2] P. Rawla, T. Sunkara, V. Gaduputi, Epidemiology of pancreatic Cancer: global trends, etiology and risk factors, world, J. Oncol. 10 (2019) 10–27.
[3] R.L. Siegel, K.D. Miller, A. Jemal, Cancer statistics, CA Cancer J. Clin. 70 (2020) (2020) 7–30.
[4] A. Neesse, P. Michl, K.K. Frese, C. Feig, N. Cook, M.A. Jacobetz, M.P. Lolkema, M. Buchholz, K.P. Olive, T.M. Gress, D.A. Tuveson, Stromal biology and therapy in pancreatic cancer, Gut 60 (2011) 861–868.
[5] C. Liang, S. Shi, Q. Meng, D. Liang, S. Ji, B. Zhang, Y. Qin, J. Xu, Q. Ni, X. Yu, Complex roles of the stroma in the intrinsic resistance to gemcitabine in pancreatic cancer: where we are and where we are going, Exp. Mol. Med. 49 (12) (2017) e406, https://doi.org/10.1038/emm.2017.255. PMID: 29611542; PMCID: PMC5750480.
[6] S.K. Dougan, The pancreatic Cancer microenvironment, Cancer J. 23 (2017).
[7] V.M. Perez, J.F. Kearney, J.J. Yeh, The PDAC extracellular matrix: a review of the ECM protein composition, Tumor Cell Interaction, and Therapeutic Strategies, Front. Oncol. 11 (2021), 751311.
[8] T. Murakami, Y. Hiroshima, R. Matsuyama, Y. Homma, R.M. Hoffman, I. Endo, Role of the tumor microenvironment in pancreatic cancer, Ann. Gastroenterol. Surgery 3 (2019) 130–137.
[9] D. von Ahrens, T.D. Bhagat, D. Nagrath, A. Maitra, A. Verma, The role of stromal cancer-associated fibroblasts in pancreatic cancer, J. Hematol. Oncol. 10 (2017) 76.
[10] T.R. Spivak-Kroizman, G. Hostetter, R. Posner, M. Aziz, C. Hu, M.J. Demeure, D. Von Hoff, S.R. Hingorani, T.B. Palculict, J. Izzo, G.M. Kiriakova, M. Abdelmelek, G. Bartholomeusz, B.P. James, G. Powis, Hypoxia triggers hedgehog-mediated tumor-stromal interactions in pancreatic cancer, Cancer Res. 73 (2013) 3235–3247.
[11] P.A. Bissey, P. Mathot, C. Guix, M. Jasmin, I. Goddard, C. Costechareyre, N. Gadot, J.G. Delcros, S.M. Mali, R. Fasan, A.P. Arrigo, R. Dante, G. Ichim, P. Mehlen, J. Fombonne, Blocking SHH/patched interaction triggers tumor growth inhibition through patched-induced apoptosis, Cancer Res. 80 (2020) 1970–1980.
[12] K.P. Olive, M.A. Jacobetz, C.J. Davidson, A. Gopinathan, D. McIntyre, D. Honess, B. Madhu, M.A. Goldgraben, M.E. Caldwell, D. Allard, K.K. Frese, G. Denicola, C. Feig, C. Combs, S.P. Winter, H. Ireland-Zecchini, S. Reichelt, W.J. Howat, A. Chang, M. Dhara, L. Wang, F. Rückert, R. Grützmann, C. Pilarsky, K. Izeradjene, S.R. Hingorani, P. Huang, S.E. Davies, W. Plunkett, M. Egorin, R.H. Hruban, N. Whitebread, K. McGovern, J. Adams, C. Iacobuzio-Donahue, J. Griffiths, D. A. Tuveson, Inhibition of hedgehog signaling enhances delivery of chemotherapy in a mouse model of pancreatic cancer, Science 324 (2009) 1457–1461.
[13] B.Y. Yan, B.P. Hibler, T. Menge, L. Dunn, A.L. Ho, A.M. Rossi, Sonic hedgehog pathway inhibitors: from clinical trials to clinical practice, Br. J. Dermatol. 180 (2019) 1260–1261.
[14] J. Berlin, J.C. Bendell, L.L. Hart, I. Firdaus, I. Gore, R.C. Hermann, M.F. Mulcahy, M.M. Zalupski, H.M. Mackey, R.L. Yauch, R.A. Graham, G.L. Bray, J.A. Low, A randomized phase II trial of Vismodegib versus placebo with FOLFOX or FOLFIRI and Bevacizumab in patients with previously untreated metastatic colorectal Cancer, Clin. Cancer Res. 19 (2013) 258–267.
[15] D.V.T. Catenacci, M.R. Junttila, T. Karrison, N. Bahary, M.N. Horiba, S.R. Nattam, R. Marsh, J. Wallace, M. Kozloff, L. Rajdev, D. Cohen, J. Wade, B. Sleckman, H.-J. Lenz, P. Stiff, P. Kumar, P. Xu, L. Henderson, N. Takebe, R. Salgia, X. Wang, W. M. Stadler, F.J. de Sauvage, H.L. Kindler, Randomized Phase Ib/II Study of Gemcitabine Plus Placebo or Vismodegib, a Hedgehog Pathway Inhibitor, in Patients With Metastatic Pancreatic Cancer, J. Clin. Oncol. 33 (2015) 4284–4292.
[16] J. Zhao, H. Wang, C.-H. Hsiao, D.S.-L. Chow, E.J. Koay, Y. Kang, X. Wen, Q. Huang, Y. Ma, J.A. Bankson, S.E. Ullrich, W. Overwijk, A. Maitra, D. Piwnica-Worms, J. B. Fleming, C. Li, Simultaneous inhibition of hedgehog signaling and tumor proliferation remodels stroma and enhances pancreatic cancer therapy, Biomaterials 159 (2018) 215–228.
[17] A.D. Rhim, P.E. Oberstein, D.H. Thomas, E.T. Mirek, C.F. Palermo, S.A. Sastra, E. N. Dekleva, T. Saunders, C.P. Becerra, I.W. Tattersall, C.B. Westphalen, J. Kitajewski, M.G. Fernandez-Barrena, M.E. Fernandez-Zapico, C. Iacobuzio-

Donahue, K.P. Olive, B.Z. Stanger, Stromal elements act to restrain, rather than support, pancreatic ductal adenocarcinoma, Cancer Cell 25 (2014) 735–747.
[18] E. Mathew, Y. Zhang, A.M. Holtz, K.T. Kane, J.Y. Song, B.L. Allen, M. Pasca di Magliano, Dosage-dependent regulation of pancreatic cancer growth and angiogenesis by hedgehog signaling, Cell Rep. 9 (2014) 484–494.
[19] M. Karaca, R. Dutta, Y. Ozsoy, R.I. Mahato, Micelle mixtures for Coadministration of gemcitabine and GDC-0449 to treat pancreatic Cancer, Mol. Pharm. 13 (2016) 1822–1832.
[20] M. Vallet-Regí, M. Colilla, I. Izquierdo-Barba, M. Manzano, Mesoporous silica nanoparticles for drug delivery: current insights, Molecules 23 (2017).
[21] R.M. Sábio, A.B. Meneguin, T.C. Ribeiro, R.R. Silva, M. Chorilli, New insights towards mesoporous silica nanoparticles as a technological platform for chemotherapeutic drugs delivery, Int. J. Pharm. 564 (2019) 379–409.
[22] R.K. Kankala, Y.H. Han, J. Na, C.H. Lee, Z. Sun, S.B. Wang, T. Kimura, Y.S. Ok, Y. Yamauchi, A.Z. Chen, K.C. Wu, Nanoarchitectured structure and surface biofunctionality of Mesoporous silica nanoparticles, Adv. Mater. 32 (2020), e1907035.
[23] J.L. Vivero-Escoto, M. Elnagheeb, Mesoporous silica nanoparticles loaded with Cisplatin and Phthalocyanine for combination chemotherapy and photodynamic therapy, Nanomaterials (Basel) 5 (2015) 2302–2316.
[24] M.P. Alvarez-Berríos, N. Sosa-Cintron, M. Rodriguez-Lugo, R. Juneja, J.L. Vivero-Escoto, Hybrid Nanomaterials based on Iron oxide nanoparticles and Mesoporous silica nanoparticles: overcoming challenges in current Cancer treatments, J. Chem. 2016 (2016) 2672740.
[25] R. Juneja, H. Vadarevu, J. Halman, M. Tarannum, L. Rackley, J. Dobbs, J. Marquez, M. Chandler, K. Afonin, J.L. Vivero-Escoto, Combination of nucleic acid and Mesoporous silica nanoparticles: optimization and therapeutic performance in vitro, ACS Appl. Mater. Interfaces 12 (2020) 38873–38886.
[26] M. Tarannum, M.A. Hossain, B. Holmes, S. Yan, P. Mukherjee, J.L. Vivero-Escoto, Advanced Nanoengineering approach for target-specific, spatiotemporal, and Ratiometric delivery of gemcitabine-Cisplatin combination for improved therapeutic outcome in pancreatic Cancer, Small 18 (2022), e2104449.
[27] M. Chiaravalli, M. Reni, E.M. O'Reilly, Pancreatic ductal adenocarcinoma: state-of-the-art 2017 and new therapeutic strategies, Cancer Treat. Rev. 60 (2017) 32–43.
[28] M.A. Moufarij, D.R. Phillips, C. Cullinane, Gemcitabine potentiates cisplatin cytotoxicity and inhibits repair of cisplatin-DNA damage in ovarian cancer cell lines, Mol. Pharmacol. 63 (2003) 862–869.
[29] Y. Tang, Y. Wang, X. Teng, Sequence-dependent effect of gemcitabine and cisplatin on A549 non-small-cell lung cancer cells, Mol. Med. Rep. 8 (2013) 221–226.
[30] O.G. Besançon, G.A. Tytgat, R. Meinsma, R. Leen, J. Hoebink, G.V. Kalayda, U. Jaehde, H.N. Caron, A.B. van Kuilenburg, Synergistic interaction between cisplatin and gemcitabine in neuroblastoma cell lines and multicellular tumor spheroids, Cancer Lett. 319 (2012) 23–30.
[31] H. Meng, Y. Zhao, J. Dong, M. Xue, Y.S. Lin, Z. Ji, W.X. Mai, H. Zhang, C.H. Chang, C.J. Brinker, J.I. Zink, A.E. Nel, Two-wave nanotherapy to target the stroma and optimize gemcitabine delivery to a human pancreatic cancer model in mice, ACS Nano 7 (2013) 10048–10065.
[32] J. Zhao, C. Wu, J. Abbruzzese, R.F. Hwang, C. Li, Cyclopamine-loaded core-cross-linked polymeric micelles enhance radiation response in pancreatic cancer and pancreatic stellate cells, Mol. Pharm. 12 (2015) 2093–2100.
[33] M. Xu, L. Li, Z. Liu, Z. Jiao, P. Xu, X. Kong, H. Huang, Y. Zhang, ABCB2 (TAP1) as the downstream target of SHH signaling enhances pancreatic ductal adenocarcinoma drug resistance, Cancer Lett. 333 (2013) 152–158.
[34] D. Ansari, M.P. Bauden, A. Sasor, C. Gundewar, R. Andersson, Analysis of MUC4 expression in human pancreatic cancer xenografts in immunodeficient mice, Anticancer Res. 34 (2014) 3905–3910.
[35] B. Manjunatha, A. Agrawal, V. Shah, Histopathological evaluation of collagen fibers using picrosirius red stain and polarizing microscopy in oral squamous cell carcinoma, J. Cancer Res. Ther. 11 (2015) 272–276.
[36] C. Han, T. Liu, R. Yin, Biomarkers for cancer-associated fibroblasts, Biomarker Res. 8 (2020) 64.
[37] J. Paulsson, P. Micke, Prognostic relevance of cancer-associated fibroblasts in human cancer, Semin. Cancer Biol. 25 (2014) 61–68.
[38] Z. Li, Y. Zhang, N. Feng, Mesoporous silica nanoparticles: synthesis, classification, drug loading, pharmacokinetics, biocompatibility, and application in drug delivery, Expert Opin. Drug Deliv. 16 (2019) 219–237.
[39] D. Dréau, L.J. Moore, M.P. Alvarez-Berrios, M. Tarannum, P. Mukherjee, J. L. Vivero-Escoto, Mucin-1-antibody-conjugated Mesoporous silica nanoparticles for selective breast Cancer detection in a Mucin-1 transgenic murine mouse model, J. Biomed. Nanotechnol. 12 (2016) 2172–2184.
[40] P. Dogra, N.L. Adolphi, Z. Wang, Y.S. Lin, K.S. Butler, P.N. Durfee, J.G. Croissant, A. Noureddine, E.N. Coker, E.L. Bearer, V. Cristini, C.J. Brinker, Establishing the effects of mesoporous silica nanoparticle properties on in vivo disposition using imaging-based pharmacokinetics, Nat. Commun. 9 (2018) 4551.
[41] G.J. Dugbartey, L.J. Peppone, I.A. de Graaf, An integrative view of cisplatin-induced renal and cardiac toxicities: molecular mechanisms, current treatment challenges and potential protective measures, Toxicology 371 (2016) 58–66.